Featured in Physics

Interacting Polaron-Polaritons

Li Bing Tan,[1,*] Ovidiu Cotlet,[1] Andrea Bergschneider,[1] Richard Schmidt,[2,3] Patrick Back,[1] Yuya Shimazaki,[1] Martin Kroner,[1] and Ataç İmamoğlu[1,†]

[1]*Institute for Quantum Electronics, ETH Zürich, CH-8093 Zürich, Switzerland*
[2]*Max Planck Institute of Quantum Optics, 85748 Garching, Germany*
[3]*Munich Center for Quantum Science and Technology, Schellingstrasse 4, 80799 Münich, Germany*

(Received 21 October 2019; revised manuscript received 19 January 2020; accepted 19 February 2020; published 15 April 2020)

Two-dimensional semiconductors provide an ideal platform for exploration of linear exciton and polariton physics, primarily due to large exciton binding energy and strong light-matter coupling. These features, however, generically imply reduced exciton-exciton interactions, hindering the realization of active optical devices such as lasers or parametric oscillators. Here, we show that electrical injection of itinerant electrons into monolayer molybdenum diselenide allows us to overcome this limitation: dynamical screening of exciton-polaritons by electrons leads to the formation of new quasiparticles termed polaron-polaritons that exhibit unexpectedly strong interactions as well as optical amplification by Bose-enhanced polaron-electron scattering. To measure the nonlinear optical response, we carry out time-resolved pump-probe measurements and observe polaron-polariton interaction enhancement by a factor of 50 (0.5 μeV μm^2) as compared to exciton-polaritons. Concurrently, we measure a spectrally integrated transmission gain of the probe field of $\gtrsim 2$ stemming from stimulated scattering of polaron-polaritons. We show theoretically that the nonequilibrium nature of optically excited quasiparticles favors a previously unexplored interaction mechanism stemming from a phase-space filling in the screening cloud, which provides an accurate explanation of the strong repulsive interactions observed experimentally. Our findings show that itinerant electron-exciton interactions provide an invaluable tool for electronic manipulation of optical properties, demonstrate a new mechanism for dramatically enhancing polariton-polariton interactions, and pave the way for realization of nonequilibrium polariton condensates.

DOI: 10.1103/PhysRevX.10.021011

Subject Areas: Condensed Matter Physics, Quantum Physics, Semiconductor Physics

I. INTRODUCTION

Monolayer transition metal dichalcogenides (TMDs) combine strong light-matter coupling and a large number of degrees of freedom with which to manipulate photons. Because of the strong Coulomb interaction, excitons constitute the elementary optical excitation and dominate optical spectra in TMDs. Many novel features of linear optical properties of TMD excitons have been demonstrated, including the optical control of the valley degrees of freedom using the helicity of the excitation light [1,2] or external magnetic fields [3–5], electrical control of the optical spectrum through injection of itinerant electrons or holes [6], and the realization of atomically thin mirrors [7,8]. However, nonlinear optical properties, crucial for the realization of novel photonic devices ranging from parametric oscillators to exciton-polariton lasers, have been largely missing in the reported studies. This is at a first glance not surprising since nonlinearities typically scale as the exciton Bohr radius and hence are suppressed in TMD monolayers where excitons are strongly bound [6,9,10], as compared to quasi-2D materials such as gallium arsenide (GaAs) quantum wells. Consequently, an outstanding challenge for the field is to find ways to enhance the exciton-exciton interaction strength, or more precisely, its ratio to the exciton radiative decay rate. Theoretical proposals to date include the exploitation of large interactions between Rydberg excitons with three-level driving schemes [11] and the reduction of the exciton radiative decay rate by placing a monolayer in a high quality-factor (Q) cavity [12] or, more elegantly, by placing a monolayer at $\lambda/2$ distance away from a mirror [13]. However, experiments have so far only confirmed that exciton-exciton interactions in neutral TMD monolayers are more than an order of magnitude weaker than those in GaAs [8,14].

*tanli@phys.ethz.ch
†imamoglu@phys.ethz.ch

In this work, we demonstrate that the presence of itinerant electrons dramatically enhances nonlinear optical properties of TMD monolayers. In an earlier work, we investigated the linear optics of doped monolayer $MoSe_2$ and identified exciton-polarons as the relevant quasiparticles [15–17]. In TMD monolayers, the exciton has an ultralarge binding energy that dominates over the electron plasma frequency and Fermi energy. In consequence, the exciton can be considered as a robust quantum impurity interacting with a fermionic bath. The itinerant electrons dynamically screen the exciton to form new quasiparticle branches—the attractive and repulsive polaron—each with a renormalized mass and energy [15,16]. A simple description of the polaron as a superposition of a bare exciton and an exciton dressed with a single electron-hole pair [18] was sufficient to accurately predict the resonances observed in linear spectroscopy. We remark that optical excitations in the presence of a 2DEG were previously analyzed both theoretically and experimentally, where the attractive polaron resonance was termed a tetron [19] or a trion-hole pair [20,21].

Here, we use nonlinear spectroscopy to investigate the residual quasiparticle interactions in the strong cavity-coupling regime [22–26] where elementary optical excitations are polaron-polaritons [15]. We find their effective polariton-polariton interaction strength to exceed that of their undressed counterparts by up to a factor of ∼50, and we demonstrate an unexpected but unequivocal amplification of polaron-polaritons accompanying the interaction-induced blueshifts, with gain factors $\gtrsim 2$.

The enhanced nonlinearities can be attributed to residual interactions between the polaron quasiparticles. Using a wave function technique, we show how the measured repulsive interaction shift in the presence of itinerant electrons can be understood in terms of a phase-space filling (PSF) effect. Here, the strong correlations between pump-generated polaritons and electrons, that are associated with the formation of a polaron dressing cloud, lead to an effective depletion of the electronic medium. Thus, additional polaritons created by the probe cannot be screened with maximal efficiency, resulting in an increase of their energy. Already at the lowest order, our approach leads to a remarkable agreement between theory and experiment: we attribute this in part to the zero-dimensional nature of the cavity mode which ensures that the lowest-energy optically excited state of the coupled system—the lower-polaron-polariton (polaron-LP)—is effectively gapped from the higher-lying continuum of polaron states, thereby suppressing higher-order interaction processes.

Residual interactions between polarons and electrons are also responsible for the observed polariton amplification [27–31]. A fraction of pump-generated polaritons contribute to the creation of a high-momentum polaron reservoir. These polarons then relax into the polaron-LP state [32,33] by generating additional electron-hole pair excitations in the electron system. In the presence of a seed population in the polaron-LP state, this scattering process is Bose enhanced [34,35], leading to the observed gain.

After describing the experimental setup and reviewing the linear optical properties in the presence of nonperturbative coupling between excitons and the cavity mode as well as excitons and electrons in Sec. II, we present the experimental signatures unveiled in nonlinear spectroscopy, namely the enhancement of nonlinearities (Sec. III) and polariton amplification in the presence of itinerant electrons as compared to the charge neutral regime (Sec. IV). We then present the theoretical model and calculations of the scattering rates due to residual interactions in Sec. V. Finally, in Sec. VI, we discuss avenues for further work.

II. ELEMENTARY OPTICAL EXCITATIONS OF AN ELECTRON-DOPED MONOLAYER $MoSe_2$ EMBEDDED IN A MICROCAVITY

Our experiments are based on a van der Waals heterostructure consisting of a $MoSe_2$ monolayer semiconductor embedded between 2 hexagonal boron nitride (*h*-BN) flakes. A top graphene layer allows us to control the electron density [Fig. 1(a)]. We place the heterostructure in a tunable zero-dimensional open cavity [36] consisting of a flat distributed-Bragg-reflector- (DBR) coated transparent substrate and a concave DBR-coated fiber facet [Fig. 1(b)] ($Q \simeq 1800$). All experiments are carried out at liquid helium temperature (see the Appendix A).

Figures 1(c) and 1(d) show the white light transmission spectrum measured for vanishing electron density ($V_g = -30$ V) and finite electron density ($V_g = 5$ V), respectively, in the strong-coupling regime as a function of the cavity length. In both cases, the measured spectra exhibit avoided crossings associated with the formation of half-light, half-matter quasiparticles termed polaritons [15,37]. In the charge neutral regime at $V_g = -30$ V, we observe an exciton-polariton normal mode splitting of 14 meV. When the monolayer is electron doped ($V_g = 5$ V), dynamical screening of the excitons by electrons dramatically alters the nature of elementary optical excitations, leading to the appearance of attractive and repulsive exciton-polaron resonances.

To analyze how the exciton-electron interaction modifies the ground state of the cavity-coupled system, we start from the Hamiltonian $H = H_{\mathrm{xe}} + H_{\mathrm{cav}}$, which can be written as

$$H_{\mathrm{xe}} = \sum_{\mathbf{k}} \omega_{\mathbf{k}} x_{\mathbf{k}}^{\dagger} x_{\mathbf{k}} + \sum_{\mathbf{k}} \epsilon_{\mathbf{k}} e_{\mathbf{k}}^{\dagger} e_{\mathbf{k}} + \frac{v}{\mathcal{A}} \sum_{\mathbf{k},\mathbf{k}',\mathbf{q}} x_{\mathbf{k}+\mathbf{q}}^{\dagger} x_{\mathbf{k}} e_{\mathbf{k}'-\mathbf{q}}^{\dagger} e_{\mathbf{k}'}, \tag{1}$$

$$H_{\mathrm{cav}} = \sum_{\mathbf{k}} \nu_{\mathbf{k}} c_{\mathbf{k}}^{\dagger} c_{\mathbf{k}} + \sum_{\mathbf{k}} \Omega (c_{\mathbf{k}}^{\dagger} x_{\mathbf{k}} + \mathrm{H.c.}). \tag{2}$$

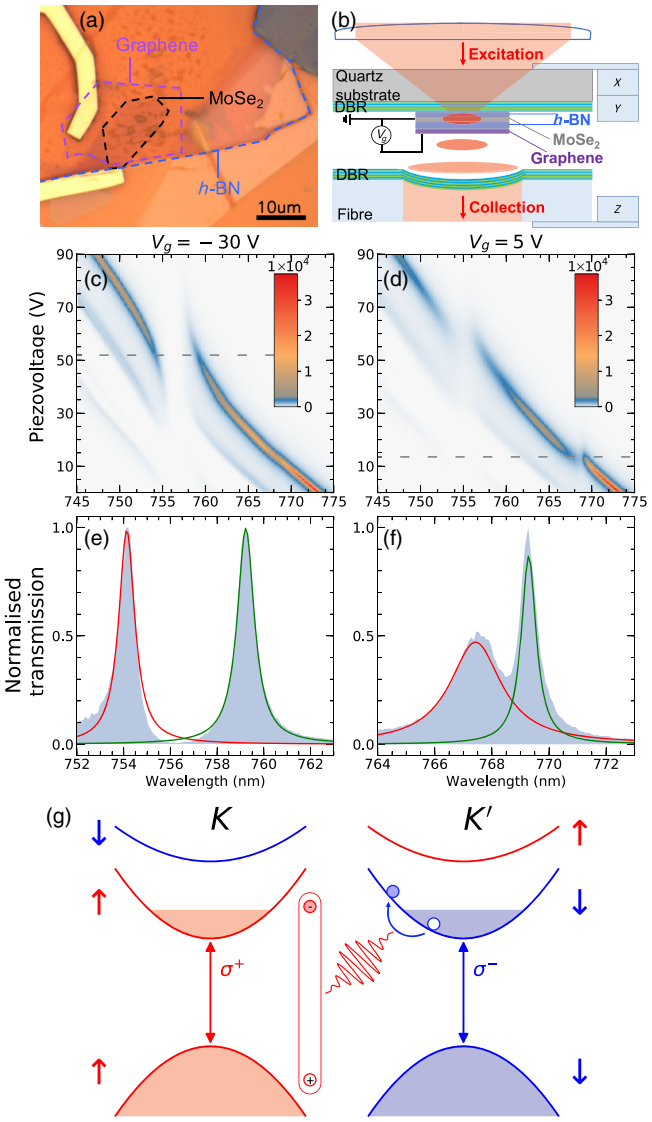

FIG. 1. Experimental setup and characterization of the sample. (a) Contrast-enhanced optical microscope image of the heterostructure. The h-BN, graphene, and $MoSe_2$ layers are indicated by dotted lines. (b) Schematic of the sample inside the cavity. The heterostructure sits on a flat dielectric mirror facing a fiber mirror which together form a cavity. The h-BN and graphene layer thicknesses are chosen such that the $MoSe_2$ lies in an antinode while the graphene lies close to a node of the cavity electric field. Applying a gate voltage between $MoSe_2$ and graphene provides electron density control. The cavity mode can be tuned *in situ* by a z-axis nanopositioner which controls the cavity length. The substrate is mounted on x- and y-axis nanopositioners which allow for in-plane translation. (c),(d) White light transmission spectrum for gate voltages $V_g = -30$ V and $V_g = 5$ V, respectively. Nonperturbative coupling between the cavity mode and optical resonances show up as anticrossings in the transmission spectrum. The faint lines originate from the higher-order cavity modes. (e),(f) Line cuts taken near the anticrossing [dashed lines in (c) and (d)] reveal the upper polariton (red) and lower polariton (green) resonances. (g) Schematic to illustrate the conduction and valence band structure and optical selection rules of monolayer $MoSe_2$ close to the K and K' points. An exciton in the K valley interacts with conduction band electron-hole pairs in the Fermi sea of the K' valley to form an intervalley polaron.

Here, $x_{\mathbf{k}}$, $e_{\mathbf{k}}$, and $c_{\mathbf{k}}$ are the annihilation operators of the exciton, electron, and cavity photon of momentum $\mathbf{k}$, respectively, with $\omega_{\mathbf{k}} = |\mathbf{k}|^2/(2m_x)$, $\epsilon_{\mathbf{k}} = |\mathbf{k}|^2/(2m_e)$, and $\nu_{\mathbf{k}} = |\mathbf{k}|^2/(2m_c) + \Delta$ their energy dispersions. The detuning Δ between cavity photons and the excitons is controlled by changing the cavity length. For numerics we use the electron mass $m_e = 0.6m_0$, the exciton mass $m_x = 2m_e$, while the cavity mass $m_c \approx 10^{-5}m_0$.

Note that in the absence of doping, the first term in Eq. (1) describes excitons as elementary excitations in the $MoSe_2$ that exhibit weak mutual residual interactions which we have chosen to neglect here. Including the second and third term takes into account the itinerant electrons and their effective interaction v with excitons when the monolayer is capacitively doped, which we model here as a contact interaction and $\mathcal{A}$ is defined as the quantization area. Equation (2) describes the effect of the cavity mode: the first term takes into account the cavity energy and the second term, which is proportional to Ω, denotes the exciton-cavity coupling.

The contact interaction v between excitons and electrons is regularized by a UV cutoff Λ. Physically, Λ can be related to the inverse Bohr radius of the exciton. However, assuming that the exciton Bohr radius is the smallest length scale in the problem, one may take $\Lambda \to \infty$ at the end of the calculation. Since any attractive interaction supports a bound state in 2D, the constant v can be related to the binding energy of the exciton-electron bound state known as the trion:

$$v^{-1} = -\frac{1}{\mathcal{A}} \sum_{|\mathbf{k}|<\Lambda} \frac{1}{E_T + \omega_{\mathbf{k}} + \epsilon_{\mathbf{k}}}, \tag{3}$$

where E_T denotes the trion binding energy.

It has been shown that the eigenstates of the interacting polariton-electron system can be accurately described using the Chevy ansatz [15]:

$$|\Psi_{\mathbf{p}}\rangle = a_{\mathbf{p}}^\dagger |\Phi\rangle = \left(\phi_{\mathbf{p}}^c c_{\mathbf{k}}^\dagger + \phi_{\mathbf{p}} x_{\mathbf{p}}^\dagger + \sum_{\mathbf{kq}} \phi_{\mathbf{pkq}} x_{\mathbf{p+q-k}}^\dagger e_{\mathbf{k}}^\dagger e_{\mathbf{q}}\right)|\Phi\rangle, \tag{4}$$

where $|\Phi\rangle$ denotes the ground state of the Fermi sea and the cavity. Note that we introduced the polaron-polariton creation operator $a_{\mathbf{p}}^\dagger$, which obeys commutation relations that are approximately bosonic. The attractive polaron oscillator strength is given by $|\phi_{\mathbf{p}}|^2$ and grows as $\sim E_F$ for low doping ($E_F < E_T$). The oscillator strength of the bare exciton is shared among the two polaron branches, ensuring the coupling of both the attractive and repulsive branch to the cavity to form polaron-polaritons with a (reduced) normal mode splitting [Fig. 1(f)].

The deviation of the exciton upper and lower polariton resonance (UP and LP) line shapes from a Lorentzian,

depicted in Fig. 1(e), stems predominantly from interference effects and indicates that polariton line broadening is primarily due to cavity losses [12]. However, the excess broadening of the polaron-UP as compared to the polaron-LP hints toward the presence of residual polaron interactions. In the following section, we describe experiments that probe the transient changes in the transmission spectrum due to the evolution of a polaron subject to these residual interactions.

We remark that due to the valley selection rules, a σ^+-(σ^--) polarized photon will excite an exciton in the K (K') valley [see Fig. 1(g)]. When the monolayer $MoSe_2$ hosts a 2DEG with a Fermi energy of ∼3.3 meV, only the lower-energy spin-split conduction band in each valley is populated. Then, a K (K') valley exciton gets dressed by electron-hole pairs formed from the Fermi sea of the K' (K) valley to form an intervalley polaron described by Eq. (4). The valley degree of freedom does not play an important role in the discussion of Sec. III but is relevant in Sec. IV.

III. ENHANCED POLARITON NONLINEARITIES DUE TO RESIDUAL QUASIPARTICLE INTERACTIONS

The time-resolved pump-probe spectroscopy setup is shown in Fig. 6. We use a spectrally narrow pump field (1 meV) with pulse duration of $\tau_{\mathrm{pump}} = 2.62 \pm 0.01$ ps to inject a majority polariton population up to as high as $n_{\mathrm{LP}} = 2 \times 10^{12}$ cm^{-2}. The probe field is spectrally broad (12 meV) with a pulse duration of $\tau_{\mathrm{probe}} = 0.3 \pm 0.1$ ps and it injects a minority polariton population in a linear orthogonal polarization unless stated otherwise. We monitor the pump-induced changes of the probe transmission as a function of time delay τ. Zero time delay ($\tau = 0$) is defined with respect to the leading edge of the pump pulse; i.e., the probe pulse impinges on the sample concurrently with the leading edge of the pump. We expect the probe transmission (i) to be unperturbed by the pump for $\tau < 0$, (ii) to show a nonlinear response due to the presence of pump-injected coherent polaritons for $0 < \tau \lesssim (\tau_{\mathrm{pol}} + \tau_{\mathrm{pump}})$, and (iii) to be modified due to interactions with a pump-induced longer-lifetime high-momentum (incoherent) polaron population for $\tau \gtrsim (\tau_{\mathrm{pol}} + \tau_{\mathrm{pump}})$.

Figure 2(a) shows a typical pump-probe measurement of the probe transmission as a function of τ. Two distinctive features are observed: a strong blueshift of the polaron-LP energy and the amplification of the probe transmission. We discuss the former in this section and the latter in the next section (Sec. IV). In the first set of experiments, we compare changes to the probe transmission in two cases: when the pump field is tuned into resonance with the exciton-LP ($n_e = 0$) and the polaron-LP transition ($n_e = 8 \times 10^{11}$ cm^{-2}, see Appendix D). The schematic is shown in the inset of Fig. 2(a).

In Figs. 2(b) and 2(c), we show the normalized transmission spectra of the probe pulse around the exciton-LP and polaron-LP resonances respectively: here, we compare the transmission for $\tau < 0$ (see dashed lines) as well as for $\tau = 2.3$ ps and $\tau = 2.7$ ps (see solid lines), the time delays at which the maximum blueshift of the exciton-LP and polaron-LP are observed. From these data, we extract ΔE_{LP}—the magnitude of the maximal LP resonance energy shift relative to its value for negative time delay. By monitoring this differential energy shift, we isolate the anharmonicity of the polariton resonance arising from interactions with the pump-field injected polaron-polaritons from cumulative changes in the optical response stemming from multiple pulse excitations that last for timescales exceeding the pulse repetition period. In Fig. 2(d), we plot ΔE_{LP} as a function of the polariton density (see Appendix C for a description of the method used to determine the polariton density). We find a dramatic enhancement of the polariton-polariton interaction strength by a factor ∼50 in the presence of itinerant electrons. Specifically, in the case of the polaron-LP, $g_{\mathrm{pp}}^{\mathrm{pol}} = 0.5\ \mu\mathrm{eV}\,\mu\mathrm{m}^2$, while for the exciton-LP, $g_{\mathrm{pp}}^{\mathrm{exc}} = 0.01\ \mu\mathrm{eV}\,\mu\mathrm{m}^2$. Our experimentally measured value for $g_{\mathrm{pp}}^{\mathrm{pol}}$ agrees with the theoretically expected value discussed in Sec. V. The bare exciton-exciton interaction strength extracted from this result is $g_{\mathrm{xx}}^{\mathrm{exc}} = 0.08\ \mu\mathrm{eV}\,\mu\mathrm{m}^2$, in agreement with earlier measurements [8,14].

For excitons, it is well understood that at low densities, nonlinearities stem mainly from Coulomb interaction. The effective exciton-exciton interaction then scales with the exciton Bohr radius a_B, which is small in TMDs compared to GaAs-based semiconductors. In contrast, for excitons that form polarons in the presence of an electronic environment, the effective interaction has two main contributions: PSF stemming from the finite electron number inside the cavity area and the exchange of an electron-hole pair between two polarons. Here, we focus on the former since we expect the latter to be negligible in the nonequilibrium case which is relevant for the description of short-lived polaritons in our experiments (see Sec. V B). The second term of Eq. (4) tells us the effective number of electron-hole pairs used from the Fermi sea to dress a single exciton impurity. As the number of impurities is increased, each successive exciton gets dressed by an increasingly depleted Fermi reservoir. This depletion of the electron reservoir has two main consequences: (1) effective blueshift of the resonance, as not as many electrons can participate in the dressing, and (2) reduction of the quasiparticle weight. The second effect shows up as a reduced oscillator strength that results in a reduction of the normal mode splitting as well as a blueshift of the LP. Consistent with the two described processes, we indeed experimentally observe both a blueshift of the polaron-LP and a reduced splitting.

We emphasize that the saturation behavior of ΔE_{LP} is observed as a function of the polariton density n_{LP} rather than the incident pump intensity. We estimate n_{LP} in a

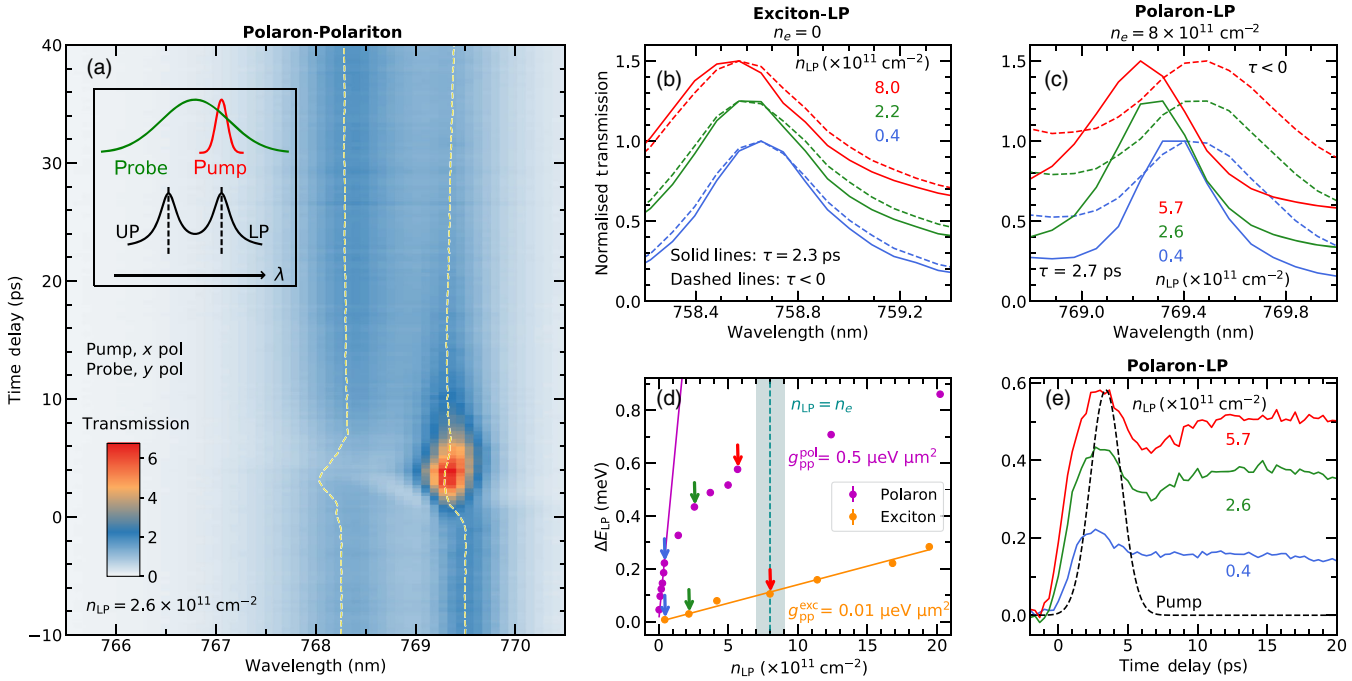

FIG. 2. Blueshift of the lower polariton due to interactions. (a) A typical time delay scan of the probe transmission spectrum from a linear cross-polarized pump-probe experiment. In this case, the polaron-lower-polariton (LP) is resonantly pumped. Inset: An illustration of the energy level scheme of the upper and lower polariton (UP and LP) branches and the pump and probe fields. The pump field is spectrally narrow and tuned in resonance to the LP while the probe field is spectrally broad and covers both branches. Yellow dashed lines show the evolution of UP and LP resonance wavelengths as a function of time delay. (b) Normalized probe transmission spectrum of the exciton-LP under resonant pumping for various polariton densities $n_{LP} = 8$, 2.1, and 0.4×10^{11} cm^{-2}. An offset has been added for clarity. Solid lines are the probe transmission spectrum measured at $\tau = 2.7$ ps. Dashed lines are the average $\tau < 0$ probe transmission spectrum obtained by taking the mean of the transmitted signal at a given wavelength over 5 different negative time delay values. (c) Analogous to (b) but for the polaron-LP at polariton densities $n_{LP} = 5.7$, 2.6, and 0.4×10^{11} cm^{-2}. (d) Energy shift of the exciton- and polaron-LP at $\tau = 2.7$ ps measured with respect to $\tau < 0$ as a function of pump power. Blue shaded area indicates the regime where polariton density and electron density are comparable in the system. The error bars are too small to be visible in the plot. For example, for the points indicated by the red arrows, the error bars are 4 and 9 μeV for the energy shift of the polaron and the exciton, respectively. (e) Evolution of the LP energy shift as a function of time delay. There is a contribution from coherent polaritons at short timescales and one from incoherent polarons at longer timescales. Black dashed line indicates the arrival of the pump pulse as determined in an independent measurement (see Appendix B).

consistent way (see Appendix C) to reflect the changes in the detuning between the lower polariton resonance and the pump energy as the intensity is changed. In doing so, we account for the change in polariton injection efficiency and remark that the observed saturation of ΔE_{LP} for the polaron-polaritons as compared to the exciton-polaritons cannot be due to the energy shifts of the polariton resonance. Rather, we attribute the saturation of the polaron-polariton energy shift to the breakdown of the polaron picture as the increasing exciton density becomes comparable to the electron density [indicated by the blue region of Fig. 2(d)]. For $n_{LP} \gtrsim 2 \times 10^{11}$ cm^{-2}, ΔE_{LP} continues to increase but with a gentler slope. In this limit, we are dealing with a Bose-Fermi mixture consisting of degenerate electrons and polaritons and we expect the simple Fermi-polaron model to be invalid.

We note that signatures of aforementioned cumulative long-timescale changes on polariton spectra are visible in the data at $\tau < 0$ [dashed lines in Fig. 2(b)]. Remarkably, while the exciton-LP for $\tau < 0$ shows a significant amount of blueshift as the excitation power is increased, the polaron-LP resonance energy remains largely unchanged. The observed blueshift of the exciton resonance at $\tau < 0$ could originate from optical doping effects due to strong pump laser illumination, effectively turning the exciton into a repulsive polaron. In contrast, in the presence of itinerant electrons, we do not expect to observe significant optical doping since the carrier density in this regime is fixed by the applied voltage.

In Fig. 2(e), we turn our attention to the time delay dependence of ΔE_{LP}. Two timescales can be seen to dominate the behavior. The resonance first blueshifts monotonically as it follows the excitation pulse shape and reaches its peak at $\tau \sim 2.7$ ps before it starts to decay, consistent with the evolution of coherent polariton population resonantly injected by the pump. Then, a second mechanism which builds up over ~12 ps takes over that eventually decays over a much longer time. The buildup of

the second peak grows noticeably more prominent as power is increased. We tentatively attribute this additional blueshift to the feeding of high-momentum polaron states from higher-energy optical excitations that are either generated by two-photon absorption or by Auger processes [38]. Since high-momentum polarons contribute to PSF as well, they also lead to a blueshift of the polaron-LP resonance. In this scenario, the rise time of the blueshift should be determined by the feeding time from higher-energy states populated by two-photon absorption and/or the Auger recombination rate, while the decay indicates the loss rate of these high-momentum polarons. For the exciton-LP, there is no clear evidence of an incoherent contribution which is likely due to the absence of itinerant carriers (see Appendix F).

IV. POLARITON GAIN

A second striking feature in Fig. 2(a) is the enhancement of the polaron-LP transmission for $2 < \tau < 6$ ps as compared to $\tau < 0$ transmission. The magnitude of the increased transmission cannot be explained by a simple change in the cavity-polaron detuning as discussed in the previous section, but rather suggests an amplification of polaritons. In Fig. 3(a), we show example line cuts for the exciton and polaron-polariton spectrum for two different τ contrasted with the typical spectrum at $\tau < 0$. We define the net transmission gain at every τ by the ratio of the integral under the shaded regions to the average integral at $\tau < 0$ (area under the dotted lines). A simple change in the cavity detuning would not lead to net gain deviating from 1 since the cavity content of the two polariton branches must always be unity. Therefore, net spectrally integrated gain exceeding unity suggests an amplification of the probe field. In semiconductor-microcavity systems, optical gain can be observed due to parametric scattering of polaritons when pumping conditions are fine-tuned such that pump, signal, and idler conserve energy and momentum [35]. However, the significant gain we observe for the polaron-LP in Fig. 3(b) considerably outlives the coherent LP population (black solid line), suggesting a contribution from a reservoir of long-lived incoherent polarons, and rules out the possibility of a coherent process as the sole mechanism.

There are a few possibilities as to how an incoherent polaron population can be generated. Firstly, due to the small normal mode splitting of the polaron-polariton, there is finite overlap of the LP with high-momentum polaron states which are not coupled to the cavity. Polarons can be created directly in high-momentum states due to the presence of disorder. Secondly, as we argued in the previous section, Auger recombination [38] or relaxation following direct two-photon absorption can efficiently populate high-momentum attractive polaron states. These states are immune to radiative decay since they lie outside the light cone and cannot recombine radiatively and satisfy

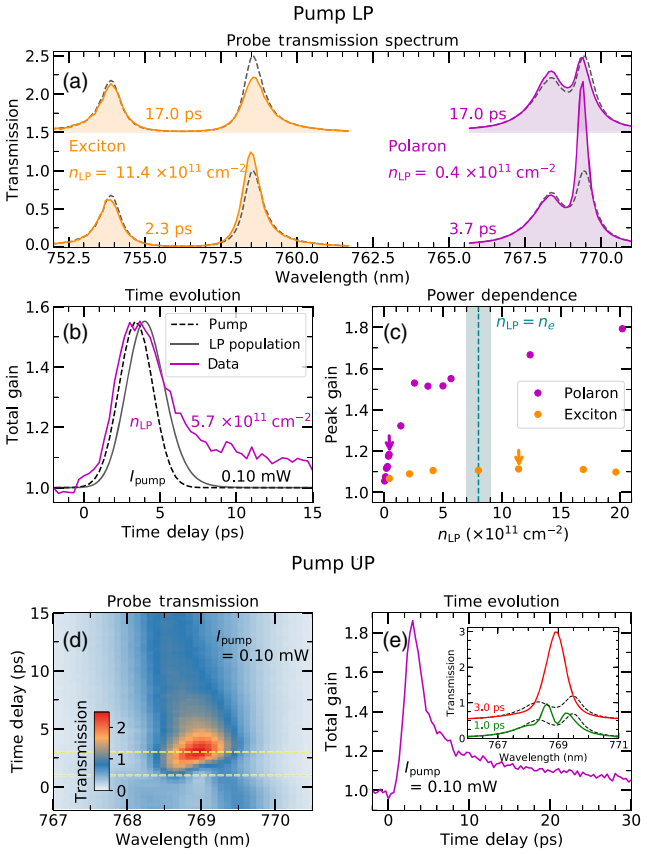

FIG. 3. Polariton amplification observed in transmission. (a) Solid lines show the probe transmission spectrum under resonant pumping of the exciton lower-polariton and polaron-LP at different time delays τ. Dashed lines show the average $\tau < 0$ probe transmission spectrum obtained by taking the mean of the transmitted signal at a given wavelength over 5 different negative time delay values. (b) Evolution of the total gain for polaron-LP as a function of τ. Gain for a given τ is calculated by dividing the integrated transmission under both UP and LP branches by the average integral taken at $\tau < 0$. Black dashed line indicates the arrival of the pump pulse as determined in an independent measurement (see Appendix B). Black solid line shows the expected time evolution of the coherent LP population injected by the pump. (c) Dependence of the peak gain on the density of LPs injected by the pump. Blue shaded area indicates the regime where polariton density and electron density are comparable in the system. (d) Time delay scan of the probe transmission spectrum for resonant pumping of the polaron-UP. (e) Time evolution of integrated gain corresponding to (d). Inset: The probe transmission spectrum at $\tau = 1$ and 3 ps indicated by yellow dashed lines in (d).

both energy and momentum conservation. We find such processes to be consistent with the second rise of the blueshift in Fig. 2(e) which grows in prominence relative to the first peak as pump power is increased. These high-momentum polarons can scatter electron-hole pairs from the Fermi sea of electrons to relax their momentum and energy into the polaron-LP state. Bose stimulation of this process due to a seed population from the probe then leads

to gain. We verified that the gain factors observed for all pump powers are independent of the incident probe power.

In Fig. 3(c), we plot the power dependence of the peak gain for the exciton- and polaron-polariton. The saturation behavior of the gain for the polaron-polariton resembles that of the blueshift: it first increases sharply and then continues with a gentler slope as n_{LP} approaches n_e. The maximum gain for the polaron-polariton is ∼1.8 while for the exciton-polariton it remains constant at 1.1 for all n_{LP}. We remark that the mechanism underlying weak exciton-polariton gain and its saturation behavior remain unclear.

In order to understand the polaron-LP gain mechanism, we studied gain under UP pumping since the population of high-momentum polarons is expected to be more efficient when pumping the UP. This is because, while the UP can relax to lower-energy, high-momentum polaron states via disorder or generation of additional Fermi sea electron-hole pairs, there are no available states for the LP to relax into (for $T < 10$ K), since it is the lowest-energy optical excitation. In Fig. 3(d), we plot the probe transmission spectrum at different τ. Gain is observed to start from the UP wavelength and redshifts with τ. However, as compared to pumping the LP, the polaron-polariton splitting collapses into a single amplified mode [inset of Fig. 3(e)], which at even longer time delays evolves into the UP resonance [Fig. 3(d)]. It is not obvious if this is due to a nonuniform gain spectrum or a breakdown of the strong-coupling regime. The peak gain when pumping the UP was found to be ∼1.8 as compared to 1.5 when pumping the LP for the same pump power [Fig. 3(e)].

Pumping the UP provides the advantage that both copolarized and cross-polarized pump-probe experiments can be done since pump photons can be filtered spectrally instead of using polarization suppression. The polarization degree of freedom is important due to valley-dependent optical selection rules in monolayer TMDs: circularly polarized photons excite polarons where excitons in a single valley are dressed by electrons in the opposite valley (as discussed at the end of Sec. II). Therefore, we expect that pump-generated reservoir polarons can only be stimulated by probe-generated LPs in the same valley. To verify this, we pump the UP with circularly polarized photons and probe with cross- and co-circularly polarized pulses. Because of spectral filtering, we limit the integration area to the LP branch when monitoring the gain. Consequently, changes in the cavity detuning can lead to gain values deviating from unity. Indeed, for circular polarization, the cross-polarized probe gain was found to be negligible as compared to its copolarized counterpart [see Fig. 4(a)]. On the other hand, the copolarized and cross-polarized probe gain are identical in linear polarization. This suggests that the gain process conserves the valley population but not the valley coherence, which is consistent with the proposed mechanism. The entanglement of polarons with the electrons during the scattering process leads to a loss of the phase relation between the valley populations.

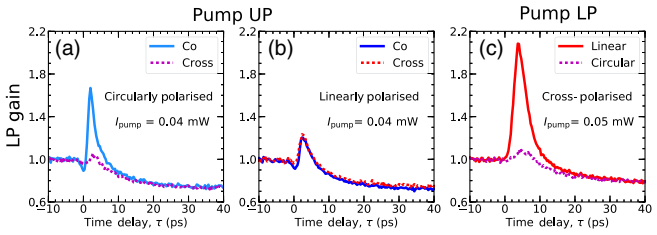

FIG. 4. Evolution of lower-polariton gain as a function of time delay τ for various pump-probe polarization configurations. LP gain for a given τ is calculated by taking the ratio of the integral under the LP branch at τ to the average integral taken at $\tau < 0$. (a) LP gain for copolarized or cross-polarized probe are plotted when resonantly pumping the polaron-UP with a circularly polarized laser. (b) Analogous to (a) but for linear polarization. (c) The polaron-LP is resonantly pumped with either linearly or circularly polarized laser while the probe is always cross-polarized.

The polarization dependence and the long-lived nature of the gain lends strong evidence for the significance of an incoherent but valley-preserving reservoir population. We also note that similar polarization-dependent behavior is observed when pumping the LP as shown in Fig. 4(c).

V. THEORETICAL MODEL

We now turn to the discussion of the theoretical model that underlies the interpretation of our experimental results. In order to model the observed phenomena theoretically, we use a wave function approach based on the Chevy ansatz given by Eq. (4). The interaction between the polarons described by this ansatz arises in our model from the symmetrization of two polaron wave functions that accounts for the underlying fermionic nature of the polaron dressing cloud. Physically this accounts for the PSF and the related depletion of the electronic medium. As outlined below, in a similar fashion, we calculate the residual interactions between polarons and electrons that lead to the decay of high-momentum polarons to the polaron-LP state, which could explain the observed gain.

Our experiments probe polariton-polariton interactions in the nonequilibrium limit where the radiative lifetime of optical excitations is comparable to or shorter than the electronic timescales, such as the disorder-induced lifetime. Since this is intrinsically a nonequilibrium problem, we have to consider interactions between polaron states that are not necessarily the lowest-energy optically excited many-body state. While a full Keldysh Green's function approach is a method of choice to analyze such non-equilibrium problems in the presence of dissipation, we show here that a wave function approach leads to remarkably good agreement between theory and experiment.

A. Fermi polaron-polaritons

The coefficients of the polaron-polariton wave function given in Eq. (4), $\phi^c_{\mathbf{p}}$, $\phi_{\mathbf{p}}$, and $\phi_{\mathbf{pkq}}$, are determined by the

minimization of $\langle\Phi|a_{\mathbf{p}}(H-E_{\mathbf{p}})a_{\mathbf{p}}^{\dagger}|\Phi\rangle$, where the polaron energy $E_{\mathbf{p}}$ is a Lagrange multiplier ensuring the normalization of the wave function. Performing this minimization we obtain the following expression for the Fermi-polaron quasiparticle energy:

$$E_{\mathbf{p}}=\nu_{\mathbf{p}}+\frac{\Omega^2}{E_{\mathbf{p}}-\omega_{\mathbf{p}}-\Sigma_{\mathrm{xe}}(\mathbf{p},E_{\mathbf{p}})}. \tag{5}$$

This equation shows that the hybridization with the excitonic degrees of freedom results in a self-energy for the photon. The exciton, in turn, acquires a self-energy Σ_{xe} due to its interactions with the electron. These interactions are renormalized from the contact potential v and determined by the electron-exciton scattering T matrix that accounts for effects of the finite electron density:

$$T(\mathbf{p},\omega)^{-1}=v^{-1}-\frac{1}{\mathcal{A}}\sum_{|\mathbf{k}|>k_F}\frac{1}{\omega-\epsilon_{\mathbf{k}}-\omega_{\mathbf{p}-\mathbf{k}}}, \tag{6}$$

where $\mathbf{p}$ and ω denote the total momentum and energy of the exciton and the electron. The self-energy is expressed in terms of the T matrix as

$$\Sigma_{\mathrm{xe}}(\mathbf{p},\omega)=\frac{1}{\mathcal{A}}\sum_{|\mathbf{q}|<k_F}T(\mathbf{p}+\mathbf{q},\omega+\epsilon_{\mathbf{q}}). \tag{7}$$

The coefficients $\phi_{\mathbf{p}}^{c}$, $\phi_{\mathbf{p}}$, and $\phi_{\mathbf{pkq}}$ can also be expressed in terms of the self-energy and the T matrix:

$$\phi_{\mathbf{p}}^{c}=\left(1-\frac{\partial}{\partial\omega}\left[\frac{\Omega^2}{\omega-\omega_{\mathbf{p}}-\Sigma_{\mathrm{xe}}(\mathbf{p},\omega)}\right]_{\omega=E_{\mathbf{p}}}\right)^{-1/2}, \tag{8}$$

$$\phi_{\mathbf{p}}=\left(1-\frac{\partial}{\partial\omega}\left[\frac{\Omega^2}{\omega-\nu_{\mathbf{p}}}+\Sigma_{\mathrm{xe}}(\mathbf{p},\omega)\right]_{\omega=E_{\mathbf{p}}}\right)^{-1/2}, \tag{9}$$

$$\phi_{\mathbf{pkq}}=\frac{T(E_{\mathbf{p}}+\epsilon_{\mathbf{q}},\mathbf{p}+\mathbf{q})\theta(|\mathbf{k}|-k_F)\theta(k_F-|\mathbf{q}|)}{E_{\mathbf{p}}-\omega_{\mathbf{p}+\mathbf{q}-\mathbf{k}}-\epsilon_{\mathbf{k}}+\epsilon_{\mathbf{q}}}\frac{\phi_{\mathbf{p}}}{\mathcal{A}}. \tag{10}$$

The terms in the square brackets in Eqs. (8) and (9) represent the photon and the exciton self-energy, respectively.

In the following, we suppress the zero-momentum label when discussing zero-momentum polarons, such that $\phi^{c}\equiv\phi_0^{c}$, $\phi\equiv\phi_0$, and $\phi_{\mathbf{kq}}\equiv\phi_{0\mathbf{kq}}$.

B. Residual interactions between polarons

For a sufficiently strong laser pump pulse, a finite polaron density is generated and interactions between the quasiparticles become important. To assess their strength, we focus here on two polarons of zero total momentum. The interaction U is given by $U/\mathcal{A}=E_2-2E_0$, where E_2 is the energy of a system with two polarons of zero total momentum and E_0 denotes the energy of a single zero-momentum polaron; we emphasize that we explicitly introduce the area factor in this expression to ensure that the interaction U has units of energy times length squared, as expected for a momentum-space interaction. To calculate E_2 we need to determine the two-polaron wave function. To first approximation the two-polaron wave function addressed by the probe pulse is given by $a_0^{\dagger}a_0^{\dagger}|\Phi\rangle$ (properly normalized). Higher-order contributions to the interaction can appear from the coupling to higher-energy states such as $a_{\mathbf{k}\neq0}^{\dagger}a_{-\mathbf{k}}^{\dagger}|\Phi\rangle$ ($k\neq0$) or states of two polarons and a number of electrons. Since these states have higher energy, they lead to attractive interactions within perturbation theory. The experimental evidence in our case shows that the interaction between polaron-polaritons is effectively repulsive, suggesting that first-order contributions dominate over higher-order interaction terms. A reason for this is the ultralow polariton mass, which ensures a large kinetic energy cost in coupling to nonzero-momentum states.

In this approximation, the strength of interaction between two polaron-LPs is given by

$$\frac{U}{\mathcal{A}}=\frac{\langle\Phi|a_0a_0Ha_0^{\dagger}a_0^{\dagger}|\Phi\rangle}{\langle\Phi|a_0a_0a_0^{\dagger}a_0^{\dagger}|\Phi\rangle}-2E_0. \tag{11}$$

Here, the overlap $\langle\Phi|a_0a_0a_0^{\dagger}a_0^{\dagger}|\Phi\rangle$ accounts for the normalization of the two-polaron wave function. If polarons were ideal bosons, this overlap would be 2. By contrast, polarons are quasiparticles composed of excitons and Fermi sea electron-hole pair excitations. In this case, the calculation of the overlap takes into account the proper antisymmetrization of the electrons and holes forming the polaron. Using Wick's theorem, it follows that

$$\langle\Phi|a_0a_0a_0^{\dagger}a_0^{\dagger}|\Phi\rangle=2(1+I_h+I_e+I_{he}), \tag{12}$$

where we introduced the exchange integrals:

$$I_h=-\sum_{\mathbf{kk'q}}|\phi_{\mathbf{kq}}|^2|\phi_{\mathbf{k'q}}|^2, \tag{13}$$

$$I_e=-\sum_{\mathbf{kqq'}}|\phi_{\mathbf{kq}}|^2|\phi_{\mathbf{kq'}}|^2, \tag{14}$$

$$I_{eh}=\sum_{\mathbf{kqq'}}|\phi_{\mathbf{kq}}|^2|\phi_{\mathbf{k+q'-q,q'}}|^2. \tag{15}$$

These sums have direct physical interpretations. To illustrate this, consider an attractive polaron at some position in the sample (the zero-momentum polaron state is a superposition of such states). The exciton attracts the surrounding electrons, forming a dressing cloud which has a size roughly given by the trion Bohr radius a_T, in the limit of low electron density. This also depletes locally the Fermi sea, in a radius roughly given by the interelectron distance

$k_F^{-1} \gg a_T$. Consider now adding a second polaron in the same zero-momentum state. The depletion of the Fermi sea created by the first exciton prohibits the formation of another polaron in this region, reducing this overlap. This effect is contained in the (negative) hole exchange contribution I_h, which reduces the overlap by a factor of the order of $k_F^{-2}/\mathcal{A}$ corresponding to the probability that the two excitons are roughly within k_F^{-1} of each other. This depletion argument does not take into account the electron density increase in the immediate vicinity of the exciton, within a radius of roughly a_T. This correction is taken into account by the electron and electron + hole exchange contributions I_e and I_{eh}, which are therefore of the order of $a_T^2/\mathcal{A}$. Hence, in the limit of low electron densities, the hole exchange contribution will dominate the other contributions roughly by a factor of $1/(k_F a_T)^2$. To simplify the derivation, we therefore neglect the smaller contributions and focus only on the interaction effects due to hole exchange from now on. With this approximation, we obtain

$$\langle\Phi|a_0 a_0 a_0^\dagger a_0^\dagger|\Phi\rangle \approx 2(1+I_h). \tag{16}$$

Substituting this back into Eq. (11), we obtain

$$\frac{U}{\mathcal{A}} \approx \frac{1}{2}\langle\Phi|a_0 a_0 H a_0^\dagger a_0^\dagger|\Phi\rangle(1-I_h) - 2E_0 \tag{17}$$

$$\approx \frac{1}{2}\langle\Phi|a_0 a_0 H a_0^\dagger a_0^\dagger|\Phi\rangle - 2E_0 - 2E_0 I_h, \tag{18}$$

where we used the fact that $I_h \ll 1$ and in the second line we replaced $\frac{1}{2}\langle\Phi|a_0 a_0 H a_0^\dagger a_0^\dagger|\Phi\rangle \approx 2E_0$ in the term proportional to I_h, since corrections to this approximation are of higher order.

The remaining expectation value can be evaluated by applying Wick's theorem once again. In this calculation, the terms $-2E_0$ and $-2E_0 I_h$ cancel all the intrapolaron direct and exchange terms that appear in $\frac{1}{2}\langle\Phi|a_0 a_0 H a_0^\dagger a_0^\dagger|\Phi\rangle$. Thus, in agreement with the expectation, only the interpolaron interaction terms will contribute to the interaction U. Furthermore, the direct interpolaron interaction is zero due to number conservation. Keeping only the hole-exchange terms yields

$$\frac{U}{\mathcal{A}} \approx -\frac{2v}{\mathcal{A}}\left[\sum_{\mathbf{k}\mathbf{k}'\mathbf{q}} \phi^*_{\mathbf{k}\mathbf{q}}\phi|\phi_{\mathbf{k}'\mathbf{q}}|^2 + \sum_{\mathbf{k}\mathbf{q}\mathbf{k}'\mathbf{q}'} \phi^*_{\mathbf{k}\mathbf{q}}\phi^*_{\mathbf{k}'\mathbf{q}'}\phi_{\mathbf{k}\mathbf{q}'}\phi_{\mathbf{k}'+\mathbf{q}-\mathbf{q}',\mathbf{q}} - \sum_{\mathbf{k}\mathbf{k}'\mathbf{q}'\mathbf{q}} \phi^*_{\mathbf{k}\mathbf{q}'}\phi_{\mathbf{k}\mathbf{q}}|\phi_{\mathbf{k}'\mathbf{q}}|^2\right]. \tag{19}$$

To understand the various terms in $U/\mathcal{A}$, it is helpful to recognize that a single polaron is formed from the superposition between a bare photon $c_0^\dagger|\Phi\rangle$, an exciton $x_0^\dagger|\Phi\rangle$, and an exciton entangled with a neutral excitation in the Fermi sea $\sum_{\mathbf{k}\mathbf{q}} \phi_{\mathbf{k}\mathbf{q}} x^\dagger_{\mathbf{q}-\mathbf{k}} e^\dagger_{\mathbf{k}} e_{\mathbf{q}}|\Phi\rangle$. The strength of the hybridization between the latter two states relies on the exciton's ability to create electron-hole pair excitations in the Fermi sea. which necessarily depends on the number of electrons in the Fermi sea.

However, when the two excitons are close to each other, and one of the excitons is in the dressed state $\sum_{\mathbf{k}\mathbf{q}} \phi_{\mathbf{k}\mathbf{q}} x^\dagger_{\mathbf{q}-\mathbf{k}} e^\dagger_{\mathbf{k}} e_{\mathbf{q}}|\Phi\rangle$ while the other exciton is in the state $x_0^\dagger|\Phi\rangle$, then it will be more difficult for the second exciton to evolve into the state $\sum_{\mathbf{k}\mathbf{q}} \phi_{\mathbf{k}\mathbf{q}} x^\dagger_{\mathbf{q}-\mathbf{k}} e^\dagger_{\mathbf{k}} e_{\mathbf{q}}|\Phi\rangle$, because some of the electrons in the Fermi sea are already correlated with the first exciton. This fact is captured by the first term in the square brackets. On the other hand, if also the second exciton is in the state $\sum_{\mathbf{k}\mathbf{q}} \phi_{\mathbf{k}\mathbf{q}} x^\dagger_{\mathbf{q}-\mathbf{k}} e^\dagger_{\mathbf{k}} e_{\mathbf{q}}|\Phi\rangle$, this state will have slightly higher energy because of the Pauli blocking between the dressing clouds of the two excitons. This repulsion mechanism is captured by the last two terms, which contain the exchange corrections coming from the exciton-electron (second term) interaction and exciton-hole interaction (third term).

One can check that the last two terms go to zero as $\Lambda \to \infty$. Indeed, since $|\phi_{\mathbf{k}\mathbf{q}}| \propto 1/|\mathbf{k}|^2$ for large momenta, one can check that the first sum in the square brackets diverges logarithmically with Λ, while the others remain constant. Therefore, only the first term can compensate the logarithmic decrease of the interaction strength v as $\Lambda \to \infty$, and the interaction is given by

$$\frac{U}{\mathcal{A}} \approx -\frac{2v}{\mathcal{A}}\sum_{\mathbf{k}\mathbf{q}} \phi^*_{\mathbf{k}\mathbf{q}}\phi \sum_{\mathbf{k}'} |\phi_{\mathbf{k}'\mathbf{q}}|^2. \tag{20}$$

This expression allows us to make the connection to the intuitive picture of phase-space filling and the related polaron-induced depletion of the electronic environment. Indeed, the last summation in Eq. (20) quantifies the depletion of the Fermi sea, since $\sum_{\mathbf{k}'} |\phi_{\mathbf{k}'\mathbf{q}}|^2 = 1 - \langle\Phi|a_0 c^\dagger_{\mathbf{q}} c_{\mathbf{q}} a_0^\dagger|\Phi\rangle$. Therefore, $v\sum_{\mathbf{k}'} |\phi_{\mathbf{k}'\mathbf{q}}|^2$ denotes the change in the amplitude for creating an electron-hole pair with momenta $\mathbf{k}, \mathbf{q}$ due to the presence of the attractive polaron at zero momentum, again, making explicit the effect of a depletion-induced interaction.

We can rewrite the above interaction in terms of the T matrix using the definition for the polaron wave function introduced in Eq. (10). Using $\partial T^{-1}(\mathbf{p},\omega)/\partial\omega = (1/\mathcal{A})\sum_{|\mathbf{k}|>k_F} 1/(\omega - \omega_{\mathbf{p}-\mathbf{k}} - \epsilon_{\mathbf{k}})^2$, we obtain

$$\frac{U}{\mathcal{A}} = \frac{\phi^4}{\mathcal{A}} \sum_{|\mathbf{q}|<k_F} \left. \frac{\partial T^2(\mathbf{q},\omega)}{\partial \omega} \right|_{\omega=E_0+\epsilon_{\mathbf{q}}}. \tag{21}$$

While this expression has the same form for both exciton-polarons and polaron-polaritons, the coupling to the cavity will modify the excitonic weight ϕ and the energy of the attractive polaron E_0, leading to induced interactions of different strength for polaron-polaritons.

The resulting interaction strength is shown for parameters typical for our experiment in Fig. 5. As expected, polaron interactions increase as we decrease the Fermi energy, because they arise due to the Pauli blocking between the Fermi sea holes localized around the polarons. At the same time, we remark that interactions increase as the light-matter coupling Ω is increased, suggesting that photon nonlinearities can be increased even further by reducing the cavity length.

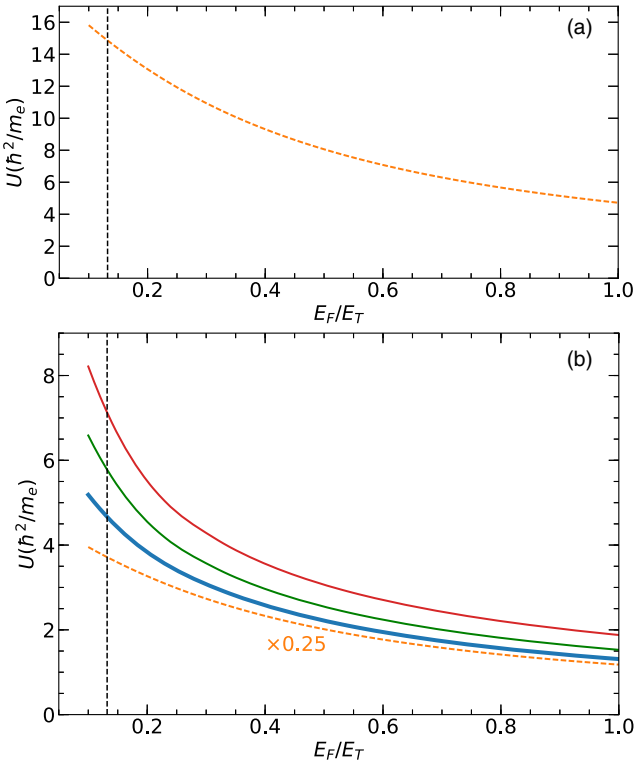

FIG. 5. (a) Interaction strength of exciton-polarons in the absence of cavity coupling. The black dashed line is a guide to the eye to illustrate the Fermi energy probed experimentally, i.e., $E_F/E_T = 3.3/25$. (b) Residual interactions between polaron-polaritons. The thicker blue line denotes the interactions of Fermi polaron-polaritons as a function of Fermi energy when $\Omega = 0.2E_T$, corresponding to the experimental value. The green and red solid lines correspond to $\Omega = 0.5E_T$ and $\Omega = 1E_T$, respectively. For this plot we choose the detuning of the cavity $\Delta = E_0 + \Omega^2/E_T$, where E_0 denotes the energy of the attractive exciton-polaron, to ensure that the polaron-polariton normal-mode splitting vanishes at zero Fermi energy. The interaction strength of exciton-polarons (scaled by a factor of 0.25) in the absence of cavity coupling has been replotted here for comparison. The enhancement of interactions with increasing cavity-polaron coupling Ω is evident. The black dashed line is a guide to the eye to illustrate the Fermi energy probed experimentally, i.e., $E_F/E_T = 3.3/25$. Energies are in units of $\hbar^2/m_e$.

For a direct comparison to the experiment we choose the parameters $E_F = 3.3$ meV, $\Omega = 5$ meV, $E_T = 25$ meV. The cavity detuning in experiments is slightly different than the detuning chosen Fig. 5. To connect to the experiments we choose $\Delta = -25$ meV, to ensure that the photonic weight of the polaron-polariton agrees with the experimental value of $|\phi^c|^2 = 0.43$, For these parameters, our theory predicts a blueshift of 0.6 μeV μm^2, which agrees remarkably well with the experimental value of 0.5 μeV μm^2.

Finally, we note that in the equilibrium limit, exchange of bosonic (electron-hole pair) excitations would provide an efficient mechanism to mediate polaron-polaron interactions [39–44]. While such a generalization of the Ruderman-Kittel-Kasuya-Yosida interactions [44–47] to the strong-coupling regime provides a pathway to strong but attractive interactions, the low energy of these bosonic excitations ensures that the mediated interactions are strongly retarded and therefore ineffective in mediating interactions between short-lived optical excitations. However, further analysis is necessary to incorporate the phase-space filling effect into a general nonequilibrium theoretical framework.

C. Polaron-electron interaction

As we argued in Sec. IV, the observed probe gain originates from the residual interactions between polarons and the Fermi sea. For simplicity, we focus here on the gain in polaron-LP when the polaron-UP branch is pumped. We envision that the relaxation of the excited polarons to polaron-LP state takes place in two sequential steps. In the first step, excitations in the polaron-UP branch decay into finite-momentum polarons by generating Fermi sea electron-hole pairs, to form a long-lived reservoir of finite-momentum polarons. In the second step, these polarons decay into the polaron-LP state by generating an additional electron-hole pair. This second process can be stimulated by a finite population in the final state, leading to net transmission gain for the probe field. Because of the complexity of the problem, we will only attempt to obtain an order-of-magnitude estimate of the gain, by calculating the rates for the two decay processes mentioned above.

The residual interactions between polarons and the Fermi sea can be estimated in an analogous way to the previous section. To this end we evaluate the matrix element:

$$\langle\Phi|e^\dagger_{\mathbf{q}}e_{\mathbf{k}}a_{\mathbf{p+q-}k}Ha^\dagger_{\mathbf{p}}|\Phi\rangle = \frac{S_{\mathbf{pkq}}}{2}(E_{\mathbf{p}}+E_{\mathbf{p+q-k}}+\epsilon_{\mathbf{k}}-\epsilon_{\mathbf{q}})+\frac{v}{\mathcal{A}}\left(\phi_{\mathbf{p}}\phi_{\mathbf{p+q-k}}+\sum_{\mathbf{k'q'}}\phi_{\mathbf{pk'q'}}\phi_{\mathbf{p+q-k,k',q'}}\right)$$
$$-\frac{v}{\mathcal{A}}\left(\sum_{\mathbf{k'q'}}\phi_{\mathbf{pk'q}}\phi_{\mathbf{p+q-k,k'q'}}+\sum_{\mathbf{k'q'}}\phi_{\mathbf{pkq'}}\phi_{\mathbf{p+q-k,k'q'}}-\frac{1}{2}\sum_{\mathbf{k'q'}}\phi_{\mathbf{pkq}}\phi_{\mathbf{p+q-k,k'q'}}-\frac{1}{2}\sum_{\mathbf{k'}}\phi_{\mathbf{pk'q}}\phi_{\mathbf{p+q-k}}\right.$$
$$\left.-\frac{1}{2}\sum_{\mathbf{q'}}\phi_{\mathbf{pkq'}}\phi_{\mathbf{p+q-k}}\right). \tag{22}$$

In the above, the term proportional to $S_{\mathbf{pkq}} \equiv \langle\Phi|e^\dagger_{\mathbf{q}}e_{\mathbf{k}}a_{\mathbf{p+q-}k}a^\dagger_{\mathbf{p}}|\Phi\rangle$ arises because we are working with a nonorthogonal basis and does not represent an interaction term. From the other terms, we focus only on the ones that remain finite in the UV limit $\Lambda\to\infty$, i.e., the second, third, and fourth terms in the last parentheses. In the low doping limit $k_F a_T \ll 1$, relevant for the description of our experiment, the fourth term dominates by a factor of $1/(k_F a_T)$, so we keep only this term, denoted by $V_{\mathbf{pkq}}$ in the following analysis. It is given by

$$V_{\mathbf{pkq}} \approx \frac{v}{2}\sum_{\mathbf{k'}}\phi_{\mathbf{pk'q}}\phi_{\mathbf{p+q-k}} \tag{23}$$
$$= \phi_{\mathbf{p}}\phi_{\mathbf{p+q-k}}T(\mathbf{p}+\mathbf{q}, E_{\mathbf{p}}+\epsilon_{\mathbf{q}}), \tag{24}$$

which agrees with previous calculations using Green's functions [48]. This matrix element describes the amplitude for the emission of an electron-hole pair with momenta $\mathbf{k}$ and $\mathbf{q}$ by a polaron of momentum $\mathbf{p}$. We emphasize that the above matrix element can also describe the residual interaction between the upper polaron-polariton and the Fermi sea, if we replace the coefficients ϕ and energy $E_{\mathbf{p}}$ with the corresponding values for the upper polaron-polariton.

To calculate the decay rate from the upper polaron-polariton into finite-momentum polaron states, we use Fermi's golden rule:

$$\Gamma^U = \sum_{\mathbf{p}}\Gamma^U_{\mathbf{p}} \equiv \sum_{\mathbf{p}}2\pi\sum_{\mathbf{q}}\left|\frac{V^U_{0,\mathbf{q-p},\mathbf{q}}}{\mathcal{A}^2}\right|^2 \times \delta(E^U_0 - E_{\mathbf{p}} - \epsilon_{\mathbf{q-p}} + \epsilon_{\mathbf{q}})\theta(k_F - |\mathbf{q}|)\theta(|\mathbf{q}-\mathbf{p}| - k_F), \tag{25}$$

where E^U_0 denotes the energy of the excited upper polaron-polariton state and we used the superscript U to emphasize that the interaction V should be evaluated using the coefficients and the energy of the upper polaron-polariton. In the above, $\Gamma_{\mathbf{p}}$ denotes the decay rate into the polaron state of momentum $\mathbf{p}$ by emission of electron-hole pairs of total momentum $-\mathbf{p}$. Choosing the same parameters as in the previous section, we obtain $\hbar\Gamma^U \approx 2$ meV. Since the radiative lifetime of polaritons is about $\hbar/(1\text{ meV})$, we conclude that pumping the upper polariton will create a sizable reservoir of finite-momentum Fermi polarons. We remark that $\Gamma_{\mathbf{p}}$ is strongly peaked at momenta $|\mathbf{p}| \sim k_F/2.5$, implying that most polarons in the reservoir will have this momentum.

We can also calculate the decay rate from a finite-momentum polaron into a lower-polaron-polariton:

$$\Gamma^L_{\mathbf{p}} = 2\pi\sum_{\mathbf{q}}\left|\frac{V_{\mathbf{p},\mathbf{p+q},\mathbf{q}}}{\mathcal{A}^2}\right|^2\delta(E_0 - E_{\mathbf{p}} - \epsilon_{\mathbf{p+q}} + \epsilon_{\mathbf{q}}). \tag{26}$$

Evaluating the above, we obtain $\Gamma^L_{k_F/2.5} \approx 1\ \mu\text{eV}\,\mu\text{m}^2/\mathcal{A}$. Assuming that the finite-momentum polaron reservoir has a population density between $n_0 = 10^{11}\text{ cm}^{-2}$ and $n_0 = 10^{12}\text{ cm}^{-2}$, we obtain a decay rate $\hbar\Gamma^L \approx N_0\Gamma^L_{k_F/2.5} = 1\ \mu\text{eV}\,\mu\text{m}^2 \times n_0$, which gives a value between 1 and 10 meV. Assuming a polariton lifetime of $\hbar/1$ meV, our simple calculation would therefore predict a net gain at polaron-LP exceeding unity, which agrees well with the experimentally observed gain.

VI. CONCLUSION

In this work, we have explored polariton-polariton interactions and Bose-enhanced scattering of polaron-polaritons in a charge-tunable $MoSe_2$ monolayer embedded in a zero-dimensional optical cavity. We found polariton-polariton interactions to be enhanced by a factor of 50 when the monolayer is electron doped as compared to the charge-neutral regime. This dramatic enhancement originates from the restriction of the oscillator strength of polarons formed within an optical spot with a fixed electron density.

Intuitively, this enhancement is a consequence of the rearrangement of the polaron dressing cloud to accommodate a larger number of optically injected impurities. In an undoped semicondutor, exciton-exciton interaction scales linearly with the Bohr radius (a_B), implying that strong light-matter coupling ($\Omega \propto 1/a_B$) is normally associated with weak nonlinearity. In stark contrast, the new mechanism we identify leads to stronger polariton interactions for stronger light-matter coupling (Fig. 4). This dependence suggests that, against expectations, strong exciton binding may even help to increase polariton-polariton interactions in electron-doped samples.

Our work further highlights the importance of time resolution when observing interaction-induced effects on polariton spectra. In particular, the measurements revealed spectral features that survive up to timescales far outliving the coherent polaritons. This observation sheds light on the

possible existence of an incoherent reservoir which contributes to the blueshift of the polaron-LP resonance that exists for timescales >10 ps. Residual polaron interactions also provide an efficient relaxation channel from these high-momentum reservoir states into the lower polariton mode, which when stimulated by probe-field injected polaritons results in optical gain. Our findings suggest that injection of itinerant electrons into a monolayer TMD could overcome the relaxation bottleneck and enable the realization of a polariton laser [34,49].

The signatures revealed by nonlinear spectroscopy in our work represent an exciting new realm of polaron physics: prior results in this field are often well described by the Chevy ansatz which models many-body dressing in terms of a single electron-hole pair. However, an accurate description of interactions that arise from the reorganization of impurity screening by the bath will require a description of higher-order exciton-electron correlations.

Furthermore, our experiments have also made a first venture into the exciting regime of degenerate Bose-Fermi mixtures where the polariton density becomes comparable to the electron density. Addressing open questions such as the electron density dependence of the onset as well as magnitude of the saturation behavior in the observed blueshift and gain will provide insight to guide theoretical understanding. While such investigations are limited in the current sample due to the normal mode splitting of the polaron-polaritons rapidly diminishing when electron density is tuned, enhancing the cavity quality factor from ∼1000 to 10 000 should allow a wider range of electron densities to be explored.

The data that support the findings of this paper are available in the ETH Research Collection [50].

ACKNOWLEDGMENTS

The authors gratefully acknowledge many enlightening discussions with Eugene Demler. We also thank Jacqueline Bloch, Georg Bruun, Jerome Faist, Meinrad Sidler, Sina Zeytinoglu, Thibault Chervy, and Ido Schwartz for useful discussions. This work is supported by a European Research Council (ERC) Advanced investigator grant (POLTDES), and by a grant from Swiss National Science Foundation (SNSF).

Note added.—Recently, a closely related work appeared [51].

APPENDIX A: SAMPLE FABRICATION AND SETUP

The monolayer $MoSe_2$, graphene, and two *h*-BN flakes were mechanically exfoliated onto SiO_2 substrates. Then they were stacked by picking up the graphene, top *h*-BN, $MoSe_2$, and the bottom *h*-BN, in that order, using a polycarbonate sacrificial layer on a polydimethylsiloxane stamp. The stack is deposited onto a fused silica substrate with a distributed Bragg reflector (DBR) coating: ten alternating layers of NB_2O_5 and SiO_2. This constitutes the planar mirror of the zero-dimensional cavity. The DBR was designed to provide >99.3% reflectivity between 680–800 nm with an intensity maximum at the DBR surface. The $MoSe_2$ and graphene flakes were contacted with Au on a 5 nm Ti sticking layer. The concave mirror was prepared by ablating a dimple of radius of curvature 30 μm onto a single-mode fiber facet which was then coated with an identical DBR as the flat substrate. After fabrication of the sample, the graphene layer was found to be torn and could not provide reliable doping. Thus, an additional graphene layer was placed on top which restored gate tunability in the sample.

The planar mirror substrate is mounted on two nanopositioners which provide in-plane spatial degrees of freedom. The fiber mirror is mounted on one nanopositioner which provides an out-of-plane degree of freedom.

APPENDIX B: OPTICAL MEASUREMENTS

The optical setup is illustrated in Fig. 6. The sample sits in a vacuum-pumped environment which is filled with 20 mbar of He exchange gas at room temperature. It is then immersed in a liquid He bath at 4.2 K for all optical measurements.

1. Pulse preparation

The output from a Ti:sapphire femtosecond pulsed laser with 76 MHz repetition rate is split into two arms: pump and probe. The pump arm is spectrally filtered with a 4*f* pulse shaping setup with a single grating. The 12 meV broad pulse is first spectrally dispersed using a transmission grating, and its spectrum selected with an adjustable slit aperture in front of a mirror and then recombined using the same grating. The probe pulse is spectrally unfiltered. Its

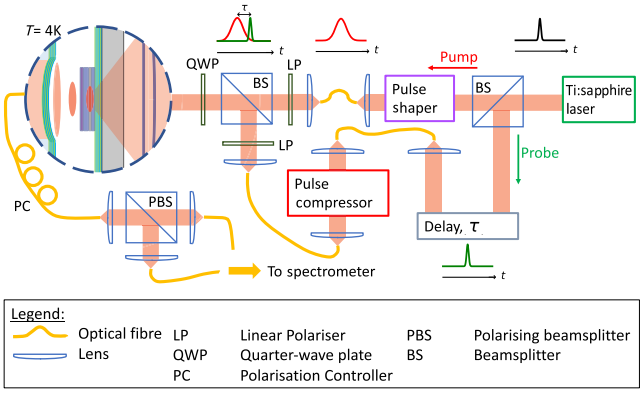

FIG. 6. A schematic of the pump-probe setup. From right to left: The output of a mode-locked Ti:sapphire laser (76 MHz repetition rate) is split into two arms: pump and probe. The pump is spectrally filtered using a pulse shaper setup. The probe pulse is sent through an optical delay line to control the time delay τ with respect to the pump pulse and a pulse compressor to compensate for linear dispersion in the optical fibers.

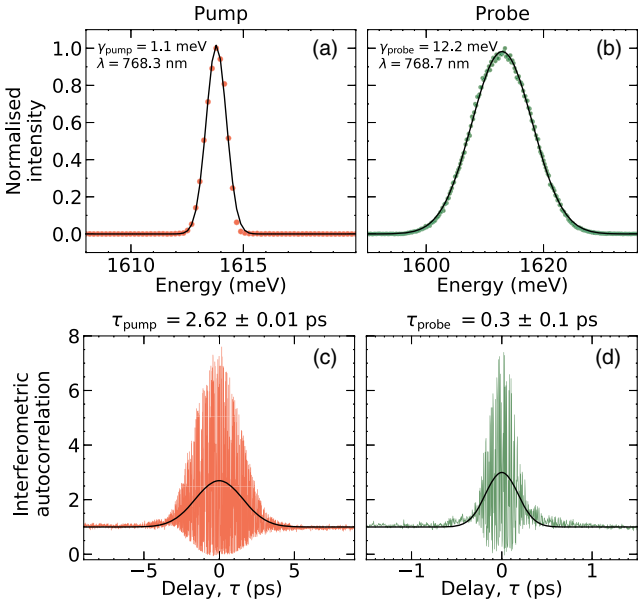

FIG. 7. (a),(b) A typical spectrum of the pump and probe pulse, respectively, after traveling through the optical fibers. (c),(d) Interferometric autocorrelation signal of the pump and probe, respectively. Black lines are Gaussian fits to the data from which the linewidths (a),(b) and pulse duration (c),(d) are extracted.

optical path length difference with respect to the pump pulse is controlled by adjusting the position of a retroreflector. In this way, the probe can be made to arrive with a variable time delay τ with respect to the pump. Both pump and probe pulses are then guided by optical fibers to the excitation arm of the transmission microscope. To avoid unwanted nonlinear effects in the fibers, we attenuate the laser powers to <1 mW before coupling them into the fibers. We check the spectrum of the pulse after traveling through the fiber in order to ensure such nonlinear effects are not present for the powers we are interested in [Figs. 7(a) and 7(b)]. In addition, there are also unwanted linear effects such as group velocity dispersion. Since the probe pulse is $\sim$12 meV broad, it is affected more significantly than the pump pulse ($\sim$1 meV). We compensate for the dispersion using a single grating pulse compressor. The pump and probe pulse durations are then measured using an interferometric autocorrelation setup in collinear geometry [Figs. 7(c) and 7(d)]. The uncertainty of the pulse durations arise from the possible deviations of the amount of dispersive elements (i.e., fiber lengths) incorporated in the autocorrelation measurement setup from the pump-probe experimental setup even as this was already taken into consideration in designing the former. We note that while we achieved significant compression of the probe, it remains not transform limited.

2. Pump-probe measurement

After the pulses are prepared, the pump and probe are coupled into the cavity via the free-space accessible side and the transmission is detected through the fiber. Using fiber polarization controllers and a polarizing beam splitter (PBS) in the detection setup, we can project the signal onto any two orthogonal polarizations. In a typical cross-polarized pump-probe measurement scheme, we measure the signal from the PBS arm that is cross-polarized with respect to the pump field using the spectrometer and, as a function of τ, we obtain the following: (i) the transmission spectrum when only the pump is turned on and (ii) the transmission spectrum when both pump and probe are turned on. In (i), we measure the cross-polarized polariton emission induced exclusively by the pump field and subtract this from (ii) in order to investigate how the transmission of the probe is influenced in the presence of the pump and as a function of τ.

3. Measurement of the zero delay between pump and probe

After mixing the pump and probe pulses with a beam splitter, the output from one port is sent to the cavity sample and the output from the second port is sent to a photodetector which measures the interfered signal. We note that the pump and probe travel through a common path after the beam splitter and, therefore, we can determine the zero delay between them as the point about which the interfered signal is symmetrical. Since this measurement is not performed *in situ* but typically done right before or after the relevant pump-probe measurements, we cannot rule out the possibility of slight drifts in the true zero-delay position over time.

APPENDIX C: POLARITON DENSITY ESTIMATION

We measure the reflection contrast of the bare cavity mode of $\eta \sim 0.13$ between resonant and off-resonant conditions. This gives an estimate of the efficiency of the coupling into the cavity. The density of intracavity polaritons per pulse is then given by $(\eta I_{\mathrm{pump}} \varepsilon / A\hbar\omega f_{\mathrm{rep}})$, where f_{rep} is the repetition rate of the pulse train, ε is the spectral overlap of the pump and the lower polariton branch, A is the area of the excitation spot, and $\hbar\omega$ is the photon energy. We are interested in the polariton density within the polariton lifetime τ_{pol}, which can be written as $(\eta I_{\mathrm{pump}} \varepsilon / A\hbar\omega f_{\mathrm{rep}}) \cdot (\tau_{\mathrm{pol}}/\tau_{\mathrm{pulse}} + \tau_{\mathrm{pol}})$.

The spectral overlap $\varepsilon(\Delta_{\mathrm{cav}})$ is in fact a function of the detuning between the cavity and the polaron (or exciton) which determines the cavity content C and the resonance of the lower polariton (or the mode being pumped) E_{LP}. Therefore, it is important to take into account the changes in ε due to blueshifts of the polaron resonance when calculating the polariton density. We want to compute ε during the pump-pulse illumination, i.e., at τ_{max} instead of at $\tau < 0$. However, when there is significant gain, it becomes difficult to determine the cavity content of the lower polariton from the area of the transmitted signal. The method we use is the following.

(1) From the polariton transmission data at $\tau < 0$, where there is no gain, we extract C and E_{LP} and calculate E_{cav} using the experimentally determined value of $\hbar\Omega$ and the expression for the Hopfield coefficient:

$$|C|^2 = \frac{1}{1 + (\frac{E_{\mathrm{LP}} - E_{\mathrm{cav}}}{\hbar\Omega})^2}, \tag{C1}$$

where $\hbar\Omega$ is the oscillator strength of the polaron.

(2) hen we extract E_{UP} and E_{LP} from the τ_{max} data where gain is observed. By taking the sum and difference of the two quantities and assuming that the cavity length remains unchanged when excited by the pump, we can find the altered oscillator strength $\hbar\Omega'$ and E'_{pol} using

$$E_{\mathrm{UP,LP}} = \frac{E_{\mathrm{cav}} + E_{\mathrm{pol}}}{2} \pm \frac{1}{2}\sqrt{(E_{\mathrm{cav}} - E_{\mathrm{pol}})^2 + 4|\hbar\Omega|^2}. \tag{C2}$$

(3) Then the cavity content at τ_{max} can be calculated using Eq. (C1).

APPENDIX D: ELECTRON DENSITY ESTIMATION

We use a capacitive model to estimate the electron density. The capacitance per unit area between the top gate and the sample is given by

$$\frac{C}{A} = \left(\frac{t}{\epsilon_0\epsilon_{h\text{-BN}}} + \frac{1}{e^2 D(E_F)}\right)^{-1}, \tag{D1}$$

where the first and second terms are the geometric and quantum capacitances, respectively. $t = (88 \pm 5)$ nm is the thickness of the h-BN flake, $\epsilon_{h\text{-BN}} = 3.5 \pm 0.5$ is the static dielectric constant of h-BN, $m^* = 0.5m_e$ is the effective electron mass in the conduction band, and $D(E_F)$ is the density of electronic states at Fermi energy E_F. For $E_F > 0$, one can neglect the quantum capacitance and write the Fermi energy as a function of applied gate voltage V_g as

$$E_F(V_g) = \frac{\pi\hbar^2\epsilon_{h\text{-BN}}\epsilon_0}{tem^*}(V_0 - V_g). \tag{D2}$$

In order to calculate the Fermi energy E_F and therefore the electron density n_e from the applied gate voltage V_g, we first need to determine the voltage V_0 at which we begin to dope the monolayer with itinerant electrons. To that end, we measured the transmission spectrum of the repulsive polaron-polariton as a function of gate voltage V_g. For small E_F (i.e., $V_g < V_0$), the Rabi splitting Ω_{rep} is given by

$$\Omega_{\mathrm{rep}}(E_F) = \sqrt{[\omega_{\mathrm{rep}}(E_F) - \omega_c]^2 + [g_{\mathrm{rep}}(E_F)]^2}, \tag{D3}$$

where $\omega_{\mathrm{rep}}(E_F) = \omega_x + \beta E_F$ is the energy of the repulsive exciton-polaron and ω_x is the exciton energy; the second term accounts for the blueshift due to the presence of the Fermi sea and β was previously found to be 0.8 [15].

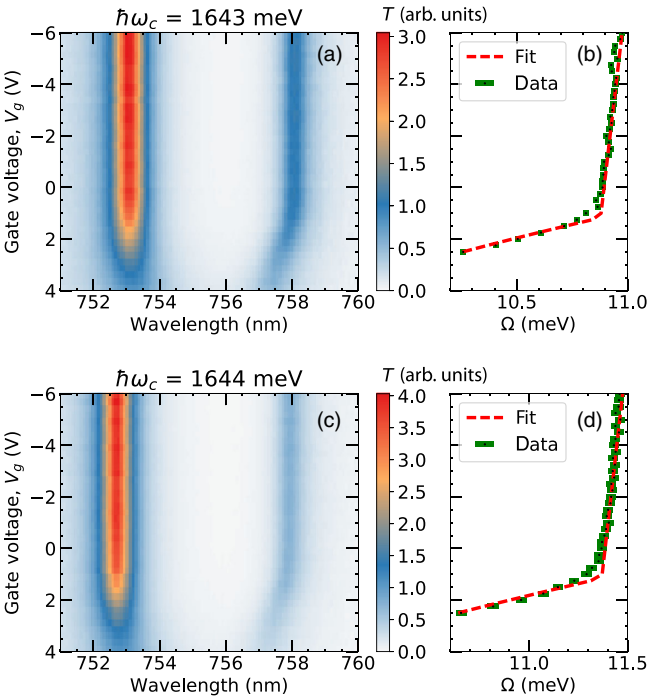

FIG. 8. (a) Transmission T spectrum of the repulsive polaron-polariton as a function of V_g at a bare cavity mode energy of $\hbar\omega_c = 1643$ meV. (b) Black dots with green error bars: Rabi splitting extracted from Lorentzian fits to the transmission spectrum. The red dashed line is a fit of the model detailed in the text to the data. (c),(d) Analogous to (a),(b) for $\hbar\omega_c = 1644$ meV.

$g_{\mathrm{rep}}(E_F)$ is the oscillator strength of the repulsive polaron, which is $\sim g_0(1 - \frac{1}{2}(E_F/E_T))$ for small E_F, E_T refers to the trion binding energy, which we take to be 25 meV.

Figures 8(a) and 8(c) show the measured transmission spectrum of the repulsive polaron-polariton for two different cavity detunings as a function of V_g. It is observed [shown in Figs. 8(b) and 8(d)] that there are two distinct regimes for the Rabi splitting Ω_{rep}. Ω_{rep} reacts much less sensitively to V_g when increasing it from -6 to ~ 1 V, after which it starts to decrease sharply. We attribute this apparent slow increase of E_F as a filling of localized states located in the midgap region resulting in a slight decrease of Ω_{rep}, which we can represent with a heuristic linear model. On the other hand, the behavior of Ω_{rep} is governed by Eq. (D3) as soon as itinerant electrons start to populate the conduction band (for $V_g > V_0$). In our fits, all parameters in Eq. (D3) were fixed except for V_0, which remained a fit parameter. We determine V_0 to be 1 V. This implies that $n_e = (8 \pm 1) \times 10^{11}$ cm^{-2} at $V_g = 5$ V. We note that the uncertainty is dominated by that of $\epsilon_{h\text{-BN}}$.

APPENDIX E: TIME DELAY DEPENDENCE OF EXCITON-POLARITON BLUESHIFT

We extract ΔE_{LP}, the magnitude of the exciton-LP resonance energy shift relative to its $\tau < 0$ value, as a

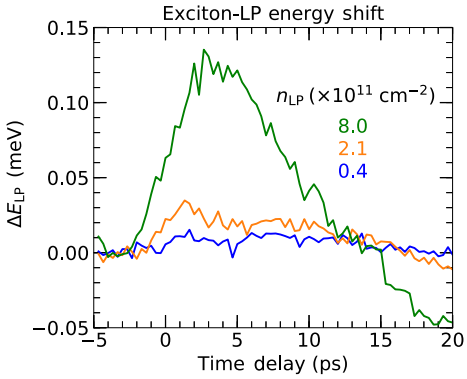

FIG. 9. Evolution of the LP energy shift as a function of time delay for different polariton densities.

function of τ in Fig. 9. We do not observe clear evidence of effects occurring after the decay of coherent polaritons.

APPENDIX F: LONG-TIMESCALE PUMP-PROBE

In the pump-probe measurements where we resonantly pump the attractive polaron-LP and the attractive polaron-UP resonantly in Figs. 2 and 3, we consistently observed a shift of the oscillator strength from the attractive polaron-LP to the UP resonance that lasted long after the gain in the transmission was over. We conducted follow-up measurements for long time-delay scans (up to 400 ps) while pumping the attractive polaron-UP. We find the timescale for the recovery of the initial conditions to be ∼300 ps (see Fig. 10).

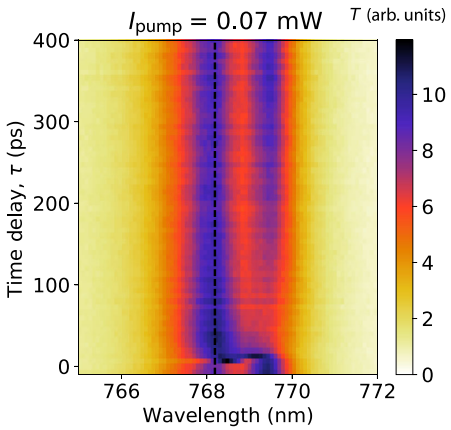

FIG. 10. Transmission (T) spectrum of the attractive polaron-polariton when resonantly pumping the UP (indicated by black dashed line) as a function of time delay τ from −10 to 400 ps at $n_e = (8 \pm 1) \times 10^{11}$ cm^{-2} and $I_{pump} = 0.07$ mW.

[1] K. F. Mak, K. He, J. Shan, and T. F. Heinz, *Control of Valley Polarization in Monolayer* MoS_2 *by Optical Helicity*, Nat. Nanotechnol. **7**, 494 (2012).

[2] H. Zeng, J. Dai, W. Yao, D. Xiao, and X. Cui, *Valley Polarization in* MoS_2 *Monolayers by Optical Pumping*, Nat. Nanotechnol. **7**, 490 (2012).

[3] A. Srivastava, M. Sidler, A. V. Allain, D. S. Lembke, A. Kis, and A. Imamoğlu, *Valley Zeeman Effect in Elementary Optical Excitations of Monolayer* WSe_2, Nat. Phys. **11**, 141 (2015).

[4] G. Aivazian, Z. Gong, A. M. Jones, R.-L. Chu, J. Yan, D. G. Mandrus, C. Zhang, D. Cobden, W. Yao, and X. Xu, *Magnetic Control of Valley Pseudospin in Monolayer* WSe_2, Nat. Phys. **11**, 148 (2015).

[5] T. Smoleński, M. Goryca, M. Koperski, C. Faugeras, T. Kazimierczuk, A. Bogucki, K. Nogajewski, P. Kossacki, and M. Potemski, *Tuning Valley Polarization in a* WSe_2 *Monolayer with a Tiny Magnetic Field*, Phys. Rev. X **6**, 021024 (2016).

[6] J. R. Schaibley, H. Yu, G. Clark, P. Rivera, J. S. Ross, K. L. Seyler, W. Yao, and X. Xu, *Valleytronics in 2D Materials*, Nat. Rev. Mater. **1**, 16055 (2016).

[7] P. Back, S. Zeytinoglu, A. Ijaz, M. Kroner, and A. Imamoglu, *Realization of an Electrically Tunable Narrow-Bandwidth Atomically Thin Mirror Using Monolayer* $MoSe_2$, Phys. Rev. Lett. **120**, 037401 (2018).

[8] G. Scuri, Y. Zhou, A. A. High, D. S. Wild, C. Shu, K. De Greve, L. A. Jauregui, T. Taniguchi, K. Watanabe, P. Kim, M. D. Lukin, and H. Park, *Large Excitonic Reflectivity of Monolayer* $MoSe_2$ *Encapsulated in Hexagonal Boron Nitride*, Phys. Rev. Lett. **120**, 037402 (2018).

[9] X. Xu, W. Yao, D. Xiao, and T. F. Heinz, *Spin and Pseudospins in Layered Transition Metal Dichalcogenides*, Nat. Phys. **10**, 343 (2014).

[10] G. Wang, A. Chernikov, M. M. Glazov, T. F. Heinz, X. Marie, T. Amand, and B. Urbaszek, *Colloquium: Excitons in Atomically Thin Transition Metal Dichalcogenides*, Rev. Mod. Phys. **90**, 021001 (2018).

[11] V. Walther, R. Johne, and T. Pohl, *Giant Optical Nonlinearities from Rydberg Excitons in Semiconductor Microcavities*, Nat. Commun. **9**, 1309 (2018).

[12] S. Zeytinoglu and A. Imamoglu, *Interaction-Induced Photon Blockade Using an Atomically Thin Mirror Embedded in a Microcavity*, Phys. Rev. A **98**, 051801(R) (2018).

[13] D. S. Wild, E. Shahmoon, S. F. Yelin, and M. D. Lukin, *Quantum Nonlinear Optics in Atomically Thin Materials*, Phys. Rev. Lett. **121**, 123606 (2018).

[14] F. Barachati, A. Fieramosca, S. Hafezian, J. Gu, B. Chakraborty, D. Ballarini, L. Martinu, V. Menon, D. Sanvitto, and S. Kena-Cohen, *Interacting Polariton Fluids in a Monolayer of Tungsten Disulfide*, Nat. Nanotechnol. **13**, 906 (2018).

[15] M. Sidler, P. Back, O. Cotlet, A. Srivastava, T. Fink, M. Kroner, E. Demler, and A. Imamoglu, *Fermi Polaron-Polaritons in Charge-Tunable Atomically Thin Semiconductors*, Nat. Phys. **13**, 255 (2017).

[16] D. K. Efimkin and A. H. MacDonald, *Many-Body Theory of Trion Absorption Features in Two-Dimensional Semiconductors*, Phys. Rev. B **95**, 035417 (2017).

[17] Y.-C. Chang, S.-Y. Shiau, and M. Combescot, *Crossover from Trion-Hole Complex to Exciton-Polaron in n-Doped Two-Dimensional Semiconductor Quantum Wells*, Phys. Rev. B **98**, 235203 (2018).

[18] F. Chevy, *Universal Phase Diagram of a Strongly Interacting Fermi Gas with Unbalanced Spin Populations*, Phys. Rev. A **74**, 063628 (2006).

[19] R. A. Suris, *Optical Properties of 2D Systems with Interacting Electrons* (Springer, New York, 2003), pp. 111–124.

[20] R. Rapaport, E. Cohen, A. Ron, E. Linder, and L. N. Pfeiffer, *Negatively Charged Polaritons in a Semiconductor Microcavity*, Phys. Rev. B **63**, 235310 (2001).

[21] F. Pulizzi, D. Sanvitto, P. C. M. Christianen, A. J. Shields, S. N. Holmes, M. Y. Simmons, D. A. Ritchie, M. Pepper, and J. C. Maan, *Optical Imaging of Trion Diffusion and Drift in GaAs Quantum Wells*, Phys. Rev. B **68**, 205304 (2003).

[22] C. Weisbuch, M. Nishioka, A. Ishikawa, and Y. Arakawa, *Observation of the Coupled Exciton-Photon Mode Splitting in a Semiconductor Quantum Microcavity*, Phys. Rev. Lett. **69**, 3314 (1992).

[23] H. Deng, H. Haug, and Y. Yamamoto, *Exciton-Polariton Bose-Einstein Condensation*, Rev. Mod. Phys. **82**, 1489 (2010).

[24] I. Carusotto and C. Ciuti, *Quantum Fluids of Light*, Rev. Mod. Phys. **85**, 299 (2013).

[25] X. Liu, T. Galfsky, Z. Sun, F. Xia, E.-c. Lin, Y.-H. Lee, S. Kéna-Cohen, and V. M. Menon, *Strong Light–Matter Coupling in Two-Dimensional Atomic Crystals*, Nat. Photonics **9**, 30EP (2015).

[26] S. Dufferwiel, S. Schwarz, F. Withers, A. A. P. Trichet, F. Li, M. Sich, O. Del Pozo-Zamudio, C. Clark, A. Nalitov, D. D. Solnyshkov, G. Malpuech, K. S. Novoselov, J. M. Smith, M. S. Skolnick, D. N. Krizhanovskii, and A. I. Tartakovskii, *Exciton–Polaritons in van der Waals Heterostructures Embedded in Tunable Microcavities*, Nat. Commun. **6**, 8579 (2015).

[27] G. Malpuech, A. Kavokin, A. Di Carlo, and J. J. Baumberg, *Polariton Lasing by Exciton-Electron Scattering in Semiconductor Microcavities*, Phys. Rev. B **65**, 153310 (2002).

[28] P. G. Lagoudakis, M. D. Martin, J. J. Baumberg, A. Qarry, E. Cohen, and L. N. Pfeiffer, *Electron-Polariton Scattering in Semiconductor Microcavities*, Phys. Rev. Lett. **90**, 206401 (2003).

[29] M. Perrin, P. Senellart, A. Lemaitre, and J. Bloch, *Polariton Relaxation in Semiconductor Microcavities: Efficiency of Electron-Polariton Scattering*, Phys. Rev. B **72**, 075340 (2005).

[30] A. I. Tartakovskii, D. N. Krizhanovskii, G. Malpuech, M. Emam-Ismail, A. V. Chernenko, A. V. Kavokin, V. D. Kulakovskii, M. S. Skolnick, and J. S. Roberts, *Giant Enhancement of Polariton Relaxation in Semiconductor Microcavities by Polariton-Free Carrier Interaction: Experimental Evidence and Theory*, Phys. Rev. B **67**, 165302 (2003).

[31] A. Qarry, G. Ramon, R. Rapaport, E. Cohen, A. Ron, A. Mann, E. Linder, and L. N. Pfeiffer, *Nonlinear Emission due to Electron-Polariton Scattering in a Semiconductor Microcavity*, Phys. Rev. B **67**, 115320 (2003).

[32] G. M. Bruun and P. Massignan, *Decay of Polarons and Molecules in a Strongly Polarized Fermi Gas*, Phys. Rev. Lett. **105**, 020403 (2010).

[33] R. Schmidt and T. Enss, *Excitation Spectra and rf Response Near the Polaron-to-Molecule Transition from the Functional Renormalization Group*, Phys. Rev. A **83**, 063620 (2011).

[34] A. Imamoglu, R. J. Ram, S. Pau, and Y. Yamamoto, *Nonequilibrium Condensates and Lasers without Inversion: Exciton-Polariton Lasers*, Phys. Rev. A **53**, 4250 (1996).

[35] P. G. Savvidis, J. J. Baumberg, R. M. Stevenson, M. S. Skolnick, D. M. Whittaker, and J. S. Roberts, *Angle-Resonant Stimulated Polariton Amplifier*, Phys. Rev. Lett. **84**, 1547 (2000).

[36] B. Besga, C. Vaneph, J. Reichel, J. Esteve, A. Reinhard, J. Miguel Sanchez, A. Imamoglu, and T. Volz, *Polariton Boxes in a Tunable Fiber Cavity*, Phys. Rev. Applied **3**, 014008 (2015).

[37] C. Schneider, M. M. Glazov, T. Korn, S. Höfling, and B. Urbaszek, *Two-Dimensional Semiconductors in the Regime of Strong Light-Matter Coupling*, Nat. Commun. **9**, 2695 (2018).

[38] B. Han, C. Robert, E. Courtade, M. Manca, S. Shree, T. Amand, P. Renucci, T. Taniguchi, K. Watanabe, X. Marie, L. E. Golub, M. M. Glazov, and B. Urbaszek, *Exciton States in Monolayer* $MoSe_2$ *and* $MoTe_2$ *Probed by Upconversion Spectroscopy*, Phys. Rev. X **8**, 031073 (2018).

[39] Z. Yu and C. J. Pethick, *Induced Interactions in Dilute Atomic Gases and Liquid Helium Mixtures*, Phys. Rev. A **85**, 063616 (2012).

[40] D. H. Santamore and E. Timmermans, *Fermion-Mediated Interactions in a Dilute Bose-Einstein Condensate*, Phys. Rev. A **78**, 013619 (2008).

[41] H. Hu, B. C. Mulkerin, J. Wang, and X.-J. Liu, *Attractive Fermi Polarons at Nonzero Temperatures with a Finite Impurity Concentration*, Phys. Rev. A **98**, 013626 (2018).

[42] A. Camacho-Guardian and G. M. Bruun, *Landau Effective Interaction between Quasiparticles in a Bose-Einstein Condensate*, Phys. Rev. X **8**, 031042 (2018).

[43] H. Tajima and S. Uchino, *Many Fermi Polarons at Nonzero Temperature*, New J. Phys. **20**, 073048 (2018).

[44] B. J. DeSalvo, K. Patel, G. Cai, and C. Chin, *Observation of Fermion-Mediated Interactions between Bosonic Atoms*, Nature (London) **568**, 61 (2019).

[45] M. A. Ruderman and C. Kittel, *Indirect Exchange Coupling of Nuclear Magnetic Moments by Conduction Electrons*, Phys. Rev. **96**, 99 (1954).

[46] T. Kasuya, *A Theory of Metallic Ferro- and Antiferromagnetism on Zener's Model*, Prog. Theor. Phys. **16**, 45 (1956).

[47] K. Yosida, *Magnetic Properties of Cu-Mn Alloys*, Phys. Rev. **106**, 893 (1957).

[48] O. Cotleţ, F. Pientka, R. Schmidt, . Zarand, and E. Demler, and A. Imamoglu, *Transport of Neutral Optical Excitations Using Electric Fields*, Phys. Rev. X **9**, 041019 (2019).

[49] M. Waldherr, N. Lundt, M. Klaas, S. Betzold, M. Wurdack, V. Baumann, E. Estrecho, A. Nalitov, E. Cherotchenko, Cai, E. A. Ostrovskaya, A. V. Kavokin, S. Tongay, S. Klembt, S. Hofling, and C. Schneider,

Observation of Bosonic Condensation in a Hybrid Monolayer $MoSe_2$-GaAs *Microcavity*, Nat. Commun. **9**, 3286 (2018).

[50] L. B. Tan, https://www.research-collection.ethz.ch/handle/20.500.11850/401640.

[51] R. P. A. Emmanuele, M. Sich, O. Kyriienko, V. Shahnazaryan, F. Withers, A. Catanzaro, P. M. Walker, F. A. Benimetskiy, M. S. Skolnick, A. I. Tartakovskii, I. A. Shelykh, and D. N. Krizhanovskii, *Highly Nonlinear Trion-Polaritons in a Monolayer Semiconductor*, arXiv:1910.14636.